MRI SATURATION

E KNOBLOCH

A. Accretion Disks vs Experiment

B. Source of energy

C. Physical Mechanisms:

reconnection / dissipation
shear profile modification
Lorentz forces
wave generation
parasitic instabilities ...

D. Saturation process is inherently nonlinear

E. Saturation process is inherently multiscale

Saturation of the Magnetorotational Instability

Edgar Knobloch
Department of Physics
University of California at Berkeley

TMBW-07, Trieste, August 2007

Collaborators:
Keith Julien, Benjamin Jamroz
Department of Applied Mathematics,
University of Colorado–Boulder.

publ's: Phys. Fluids 17, 094106 (2005); EAS Publications Series, 21 (2006); J. Math. Phys. 48, 065405 (2007).

Talk Outline

- Motivation
  - Accretion disks
  - Laboratory experiments
- Model Problem
  - Local shearing sheet approximation
- Scaling
- Asymptotic solution
- Sample solutions
- Interpretation of the solution
- Discussion

Motivation

- Turbulent accretion disks require the presence of an efficient mechanism for ang. mtm. transport
- MRI: Linear instability occurring in Rayleigh-stable regimes in the presence of a weak poloidal B-field.
  - Thin sheets of matter moving radially inwards and outwards
  - Couette-Taylor geometry: Velikhov 1959, Chandrasekhar 1960
  - Keplerian Disks: Balbus-Hawley 1991, 1998
- Efficiency of ang. mtm. transport dependent on saturation of MRI

- Numerical investigations: Shearing sheet geometry
  - Balbus-Hawley 1991: evol'n to solid body rotation, X-points suggest reconnection process importan saturation
  - Sano *et al.*1998: whether saturation occurs dependent on Elssaser number $\Lambda(> or < 1)$
  - Goodman & Xu 1994, Flemming *et al.*2000; Saturation $\forall\Lambda$ if non-axisymmetric instability included.
- Numerical investigations: Global cylindrical geometry
  - Kersale *et al.* 2004, 2006
  - Cattaneo *et al.* 2005

Motivation

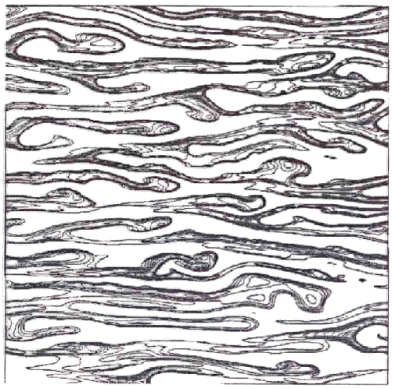

- Turbulent accretion disks require the presence of an efficient mechanism for ang. mtm. transport
- MRI: Linear instability occurring in Rayleigh-stable regimes in the presence of a weak poloidal B-field.
  - Thin sheets of matter moving radially inwards and outwards
  - Couette-Taylor geometry: Velikhov 1959, Chandrasekhar 1960
  - Keplerian Disks: Balbus-Hawley 1991, 1998
- Efficiency of ang. mtm. transport dependent on saturation of MRI

- Numerical investigations: Shearing sheet geometry
  - Balbus-Hawley 1991: evol'n to solid body rotation, X-points suggest reconnection process importan saturation
  - Sano *et al.*1998: whether saturation occurs dependent on Elssaser number $\Lambda(> or < 1)$
  - Goodman & Xu 1994, Flemming *et al.*2000; Saturation $\forall\Lambda$ if non-axisymmetric instability included.

Motivation

- Turbulent accretion disks require the presence of an efficient mechanism for ang. mtm. transport
- MRI: Linear instability occurring in Rayleigh-stable regimes in the presence of a weak poloidal B-field.
  - Thin sheets of matter moving radially inwards and outwards
  - Couette-Taylor geometry: Velikhov 1959, Chandrasekhar 1960
  - Keplerian Disks: Balbus-Hawley 1991, 1998
- Efficiency of ang. mtm. transport dependent on saturation of MRI

- Numerical investigations: Global cylindrical geometry
  - Kersale *et al.* 2004, 2006
  - Cattaneo *et al.* 2005
- Laboratory Experiments: Global cylindrical geometry
  - Sisan *et al.* 2004

Formulation of a Model Problem

- Shearing sheet approx'n at r^* with local ang velocity $\Omega^*(r^*)\hat{\mathbf{z}}$:
- Straight channel: $-L^*/2 \le x^* \le L^*/2$, $-\infty < y^* < \infty$, $-\infty < z^* < \infty$
- Linear shear: $\mathbf{U_0}^* = (0, \sigma^* x^*, 0)$
- Constant B-Field: $\mathbf{B_0}^* = (0, B^*_{tor}, B^*_{pol})$
- Perturbations: $\mathbf{u} \equiv (u, v, w) = (-\psi_z, v, \psi_x)$, $\mathbf{b} \equiv (a, b, c) = (-\phi_z, b, \phi_x)$

  Axisymmetric Equations

$$\nabla^2\psi_t + 2\Omega v_z + J(\psi, \nabla^2\psi) = v_A^2\nabla^2\phi_z + v_A^2 J(\phi, \nabla^2\phi) + \nu\nabla^4\psi, \qquad (1)$$

$$v_t - (2\Omega + \sigma)\psi_z + J(\psi, v) = v_A^2 b_z + v_A^2 J(\phi, b) + \nu\nabla^2 v, \qquad (2)$$

$$\phi_t + J(\psi, \phi) = \psi_z + \eta\nabla^2\phi, \qquad (3)$$

$$b_t + J(\psi, b) = v_z - \sigma\phi_z + J(\phi, v) + \eta\nabla^2 b, \qquad (4)$$

where $J(f, g) \equiv f_x g_z - f_z g_x$

- $v_A \equiv B^*_{pol}/\sqrt{\mu_0\rho^*}U^*$, Ω, ν, η *dimensionless* Alfvén speed, rotation rate, kinematic viscosity and ohmic diffusivity.

Remarks on Model Problem

Local shearing sheet approx'n ⇒ number of properties to model eqns

- Toroidal field B^*_{tor} drops out
  - suppression of hoop stresses
  - toroidal field remains in the radial pressure balance

$$2\Omega^* V_0^* + \frac{V_0^{*2}}{r^*} = \frac{1}{\rho^*}\frac{dP_0^*}{dr^*} + \frac{d}{dr^*}\left(\frac{B^{*2}_{tor}}{2\mu_0\rho^*}\right) + \frac{B^{*2}_{tor}}{\mu_0\rho^* r^*}, \qquad (5)$$

- No distinction btw inward and outward directions
  - symmetry $x \to -x$, $(\psi, v, \phi, b) \to -(\psi, v, \phi, b)$
  - direction of accretion and angular mtm flux must be imposed externally
- MRI is an exponentially growing instability
  - This is not the case in polar coordinates with nonzero B^*_{tor}

Linear Theory

- Linearization about the trivial state $\psi = v = \phi = b = 0$
- Perturbation $\exp[\lambda t + ikx + nz]$ and $p = k^2 + n^2 \Rightarrow$ disp'n rel'n

$$p[(\lambda+\nu p)(\lambda+\eta p)+v_A^2 n^2]^2 + 2\Omega n^2[(\lambda+\eta p)^2(2\Omega+\sigma)+\sigma v_A^2 n^2] = 0. \quad (6)$$

- Conventional view of MRI: positive growth rate λ achieved for sufficiently large vertical wavenumbers n whenever $\sigma < 0$, $v_A \neq 0$, provided only that ν, and η are sufficiently small.
  - For $\nu = \eta = 0$

$$\lambda^2 = -\frac{v_A^2 n^2 \sigma}{2\Omega + \sigma} + O(v_A^4 n^4). \quad (7)$$

  - For $\lambda = 0$ threshold for instability exists. For small ν, η critical Elsasser number

$$\Lambda_c \equiv v_A^2/\Omega\eta = \eta\left(\frac{2\Omega+\sigma}{\Omega\sigma}\right)\frac{p^2}{n^2} + O(\nu,\eta)^3. \quad (8)$$

  - Reconnection effects described by finite η are more important for stabilizing the system against the MRI than viscosity.

Scaling Assumptions

- Traditional approach to nonlinear saturation: weakly nonlinear theory with $(\Lambda - \Lambda_c)/\Lambda_c \ll 1$.
- Our approach: strongly nonlinear theory with $\Lambda \gg \Lambda_c$.
  - shear is the dominant source of energy for the MRI
  - MRI itself requires the presence of a (weaker) vertical magnetic field
  - Dissipative effects are weaker still but cannot be ignored since they are ultimately responsible for the saturation of the instability.
- Hence scalings
  - Rapid rotation, strong shear: $(\Omega, \sigma) = \epsilon^{-1}(\hat{\Omega}, \hat{\sigma})$
  - Magnetic field: $v_A = 1$ *i.e.*, $U^* = v_A^* \equiv B_{pol}^*/\sqrt{\mu_0 \rho^*}$
  - Weak dissipative processes, $(\nu, \eta) = \epsilon(\hat{\nu}, \hat{\eta})$
  - Thin fingers, strong growth: $\partial_x \to \partial_x, \quad \partial_z \to \epsilon^{-1}\partial_z, \quad \partial_t \to \epsilon^{-1}\partial_t$
- Thus $\Omega = (\Omega^*/|\sigma^*|)Rm\, S^{-1}$, $\sigma = Rm\, S^{-1}$, $\quad \eta = S^{-1}$, $\nu = Pm\, S^{-1}$, Lundquist $S \equiv v_A^* L^*/\eta^*$, M-Reynolds $Rm = |\sigma^*|L^{*2}/\eta^*$, M-Prandtl $Pm = \nu^*/\eta^*$
- Meaning of $\epsilon \ll 1$? Requirement that $Rm \gg S \gg \max(1, Pm)$.

Scaled Equations

- In parallel with the above assumptions we need to make further assumptions about the relative magnitude of the various fields.
- We find $(\psi, \phi) \to \epsilon(\psi, \phi)$, $(v, b) \to \epsilon^{-1}(v, b)$ leads to a self-consistent set of reduced pde's
- scaled pde's

$$\epsilon \frac{D}{Dt}\left(\partial_x^2 + \epsilon^{-2}\partial_z^2\right)\psi + 2\epsilon^{-3}\hat{\Omega} v_z = v_A^2\left(\partial_x^2 + \epsilon^{-2}\partial_z^2\right)\phi_z + \epsilon v_A^2 J\left(\phi, \left(\partial_x^2 + \epsilon^{-2}\partial_z^2\right)\phi\right) + \epsilon^2 \hat{\nu}\left(\partial_x^2 + \epsilon^{-2}\partial_z^2\right)^2 \psi \quad (9)$$

$$\epsilon^{-1}\frac{D}{Dt} v - \epsilon^{-1}(2\hat{\Omega} + \hat{\sigma})\psi_z = \epsilon^{-2} v_A^2 b_z + \epsilon^{-1} v_A^2 J(\phi, b) + \hat{\nu}(\partial_x^2 + \epsilon^{-2}\partial_z^2) v \quad (10)$$

$$\epsilon \frac{D}{Dt}\phi = \psi_z + \epsilon^2 \hat{\eta}(\partial_x^2 + \epsilon^{-2}\partial_z^2)\phi \quad (11)$$

$$\epsilon^{-1}\frac{D}{Dt} b = \epsilon^{-2} v_z - \epsilon^{-1}\hat{\sigma}\phi_z + \epsilon^{-1} J(\phi, v) + \hat{\eta}(\partial_x^2 + \epsilon^{-2}\partial_z^2) b \quad (12)$$

where $D/Dt = \partial_t + J[\psi, \bullet]$.

Derivation of Reduced PDE's

- To solve the scaled equations we suppose $\psi(x, z, t) = \psi_0(x, z, t) + \epsilon\psi_1(x, z, t) + \ldots$, etc.
- Deduction: Leading order azimuthal fields v_0, b_0 represent large-scale adjustment to background shear and toroidal field due to MRI
  - From Eqn's for azimuthal fields v, b at $O(\epsilon^{-2})$ and poloidal fields ψ at $O(\epsilon^{-3})$

$$v_A^2 b_{0z} + \hat{\nu} v_{0zz} = 0, \qquad v_{0z} + \hat{\eta} b_{0zz} = 0, \qquad 2\widehat{\Omega} v_{0z} = 0 \quad (13)$$

  - Hence

$$v_0 = V(x, t), \qquad b_0 = B(x, t) \quad (14)$$

  - Averaging in t at $O(\epsilon^{-1}) \Rightarrow$ slow time evolution. Hence

$$v_0 = V(x), \qquad b_0 = B(x) \quad (15)$$

Reduced PDE's

- From Eqs for azimuthal fields v, b at $O(\epsilon^{-1})$ and poloidal fields ψ, ϕ at $O(\epsilon^{-2})$, $O(1)$

$$\psi_{0zzt} + 2\widehat{\Omega} v_{1z} = v_A^2 \phi_{0zzz} + \widehat{\nu}\psi_{0zzzz} \tag{16}$$

$$v_{1t} - (2\widehat{\Omega} + \widehat{\sigma} + V'(x))\psi_{0z} = v_A^2 b_{1z} - v_A^2 B'(x)\phi_{0z} + \widehat{\nu} v_{1zz} \tag{17}$$

$$\phi_{0t} = \psi_{0z} + \widehat{\eta}\phi_{0zz} \tag{18}$$

$$b_{1t} - \psi_{0z} B'(x) = v_{1z} - (\widehat{\sigma} + V'(x))\phi_{0z} + \widehat{\eta} b_{1zz} \tag{19}$$

- Closure requires determination of $V'(x), B'(x)$.
  - Averaging Eqn's for azimuthal fields v, b at $O(1)$ in z, t and integrating gives

$$\widehat{\nu} V'(x) = \overline{\psi_0 v_{1z}} - v_A^2 \overline{\phi_0 b_{1z}} + C_1 \tag{20}$$

$$\widehat{\eta} B'(x) = \overline{\psi_0 b_{1z}} - \overline{\phi_0 v_{1z}} + C_2 \tag{21}$$

- C_1 is determined by BC's; $0 < C_2 < C_{max}$ range of total to zero support of disk by radial pressure gradient.

Strongly Nonlinear Single-Mode Solutions

These equations have stationary solutions of the form

$$\psi_0 = \frac{1}{2}(\Psi(x)\, e^{inz} + \text{c.c.}), \quad v_1 = \frac{1}{2}(\mathcal{V}(x)\, e^{inz} + \text{c.c.}), \tag{22}$$
$$\phi_0 = \frac{1}{2}(\mathcal{F}(x)\, e^{inz} + \text{c.c.}), \quad b_1 = \frac{1}{2}(\mathcal{B}(x)\, e^{inz} + \text{c.c.}),$$

where

$$\mathcal{F} = \frac{i\Psi}{\hat{\eta} n}, \tag{23}$$

$$\mathcal{V} = \frac{(v_A^2 + \hat{\eta}^2 n^2)V' + \hat{\eta}^2 n^2 (2\hat{\Omega} + \hat{\sigma}) + v_A^2 \hat{\sigma}}{n\hat{\eta}(v_A^2 + \hat{\nu}\hat{\eta} n^2)}\, i\Psi, \tag{24}$$

$$\mathcal{B} = \frac{i(v_A^2 + \hat{\nu}\hat{\eta} n^2)B' + n(\hat{\nu}(\hat{\sigma} + V') - \hat{\eta}(2\hat{\Omega} + \hat{\sigma} + V'))}{n\hat{\eta}(v_A^2 + \hat{\nu}\hat{\eta} n^2)}\, \Psi. \tag{25}$$

and we obtain the nonlinear dispersion relation

$$2\hat{\Omega}[(v_A^2 + \hat{\eta}^2 n^2)V' + (2\hat{\Omega} + \hat{\sigma})\hat{\eta}^2 n^2 + \hat{\sigma} v_A^2] + n^2 (v_A^2 + \hat{\nu}\hat{\eta} n^2)^2 = 0. \tag{26}$$

- Except for the presence of the additional shear rate V' this is nothing but the dispersion relation for the MRI in our scaling regime

Strongly Nonlinear Single-Mode Solutions

These equations have stationary solutuions of the form

$$\psi_0 = \frac{1}{2}(\Psi(x)\, e^{inz} + \text{c.c.}), \quad v_1 = \frac{1}{2}(\mathcal{V}(x)\, e^{inz} + \text{c.c.}), \tag{27}$$
$$\phi_0 = \frac{1}{2}(\mathcal{F}(x)\, e^{inz} + \text{c.c.}), \quad b_1 = \frac{1}{2}(\mathcal{B}(x)\, e^{inz} + \text{c.c.}),$$

where

$$\mathcal{F} = \frac{i\Psi}{\hat{\eta} n}, \quad \mathcal{V} = Func\left[V'; \widehat{\Omega}, \widehat{\sigma}, v_A, \widehat{\nu}, \widehat{\eta}\right] i\Psi, \quad \mathcal{B} = Func\left[V', B'; \widehat{\Omega}, \widehat{\sigma}, v_A, \widehat{\nu}, \widehat{\eta}\right] i\Psi$$

and we obtain the nonlinear dispersion relation

$$2\hat{\Omega}[(v_A^2 + \hat{\eta}^2 n^2)V' + (2\hat{\Omega} + \hat{\sigma})\hat{\eta}^2 n^2 + \hat{\sigma} v_A^2] + n^2(v_A^2 + \hat{\nu}\hat{\eta} n^2)^2 = 0. \tag{28}$$

- Except for the presence of the additional shear rate V' this is nothing but the dispersion relation for the MRI in our scaling regime
- For each wavenumber n dispersion relation determines V' (see Figure)
- Closure requires the determination of V', B' as a function of Ψ

Nonlinear Dispersion Relation

- nonlinear dispersion relation: V' =const. as function of n

$$2\hat{\Omega}[(v_A^2 + \hat{\eta}^2 n^2)V' + (2\hat{\Omega} + \hat{\sigma})\hat{\eta}^2 n^2 + \hat{\sigma} v_A^2] + n^2(v_A^2 + \hat{\nu}\hat{\eta} n^2)^2 = 0. \tag{29}$$

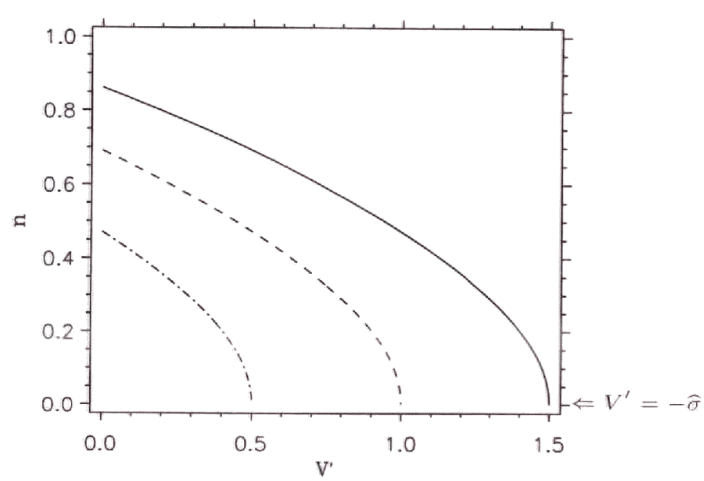

$\widehat{\Omega} = 1, v_A = 1, \widehat{\nu} = \widehat{\eta} = 1$, and $\widehat{\sigma} = -1.5, -1, -0.5$ (solid, dashed, dashed-dot)

- n decreases from its linear theory value indicating increase in the vertical wavelength as MRI saturates. Selecte n vanishes when solid body rotation reached.

Single-Mode Solutions: Closure

- Closure requires the determination of V', B' as a function of Ψ. Given

$$\psi_0 = \frac{1}{2}(\Psi(x)\, e^{inz} + \text{c.c.}), \quad v_1 = \frac{1}{2}(\mathcal{V}(x)\, e^{inz} + \text{c.c.}), \tag{30}$$
$$\phi_0 = \frac{1}{2}(\mathcal{F}(x)\, e^{inz} + \text{c.c.}), \quad b_1 = \frac{1}{2}(\mathcal{B}(x)\, e^{inz} + \text{c.c.}),$$

We find

$$V'(x) = \frac{C_1 - \frac{1}{2}\beta|\Psi|^2}{\widehat{\nu} + \frac{1}{2}\alpha|\Psi|^2}, \quad \alpha, \beta = Func\left[\widehat{\Omega}, \widehat{\sigma}, v_A, \widehat{\nu}, \widehat{\eta}\right] \tag{31}$$

$$B'(x) = \frac{\widehat{\eta} C_2}{\widehat{\eta}^2 + \frac{1}{2}|\Psi|^2} \tag{32}$$

- MRI requires $C_1 = 0$ for nonzero V' and Ψ
- Nonlinear dispersion then gives saturated value of $|\Psi|$

$$|\Psi|^2 = -\frac{2\widehat{\nu}\widehat{\eta}^2\left[n^2(v_A^2 + \widehat{\nu}\widehat{\eta}n^2)^2 + 2\widehat{\Omega}\widehat{\sigma}v_A^2 + 2\widehat{\Omega}(2\widehat{\Omega} + \widehat{\sigma})\widehat{\eta}^2 n^2\right]}{\left[4\widehat{\Omega}^2 v_A^2\widehat{\eta} + n^2\left(v_A^2 + \widehat{\nu}\widehat{\eta}n^2\right)\left(\widehat{\nu}v_A^2 + \widehat{\eta}^3 n^2\right)\right]} \tag{33}$$

  - This is a bifurcation equation with saturation determined by bifurcation parameter $\widehat{\sigma}$ or v_A (equivalently, the Elsasser number Λ)

Single Mode Results I

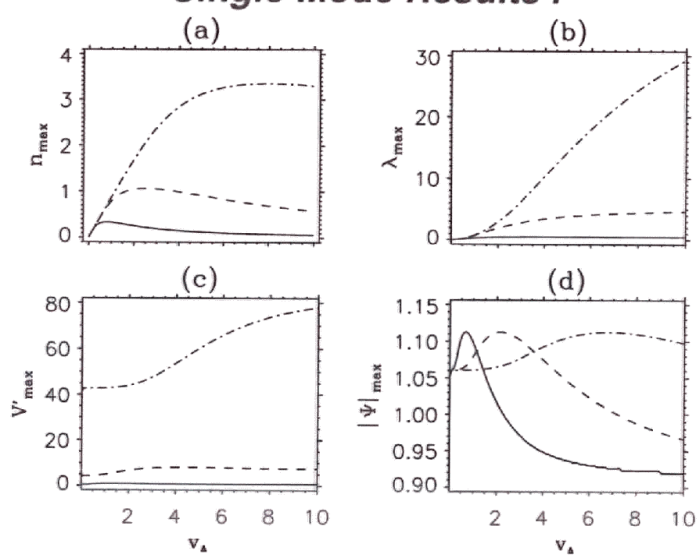

$\widehat{\Omega} = -2/3\widehat{\sigma}$, $\widehat{\nu} = \widehat{\eta} = 1$, and $\widehat{\sigma} = -100, -10, -1$ (dashed-dot, dashed, solid)

- Maximum growth rate λ and V' increases with v_A, whereas associated wavenumber n and saturation level $|\psi|$ peaks.
- Increasing n initially gets around stabilizing Lorentz force but once MRI flow is capable of slipping through th field further increases in n is of no benefit. Further increases result in additional modification of V'

Single Mode Results II

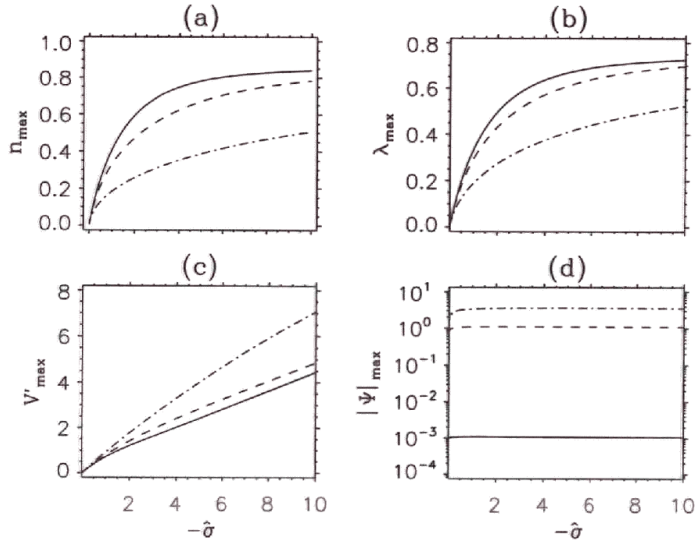

$\widehat{\Omega} = -2/3\widehat{\sigma}$, $v_A = \widehat{\eta} = 1$, and $\widehat{\nu} = 10^{-6}, 1, 10$ (solid, dashed, dashed-dot)

- V' Increases rapidly with shear rate $|\widehat{\sigma}|$ while $n, \lambda, |\Psi|$ saturates. A consequence of the weaker role played b Coriolis force.
- Saturation values increase with ν indicating subtle role of viscosity in nonlinear regime c.f. linear regime. Large viscosity transports larger ang. mtm. competing with magnetic stresses.

Single Mode Results III

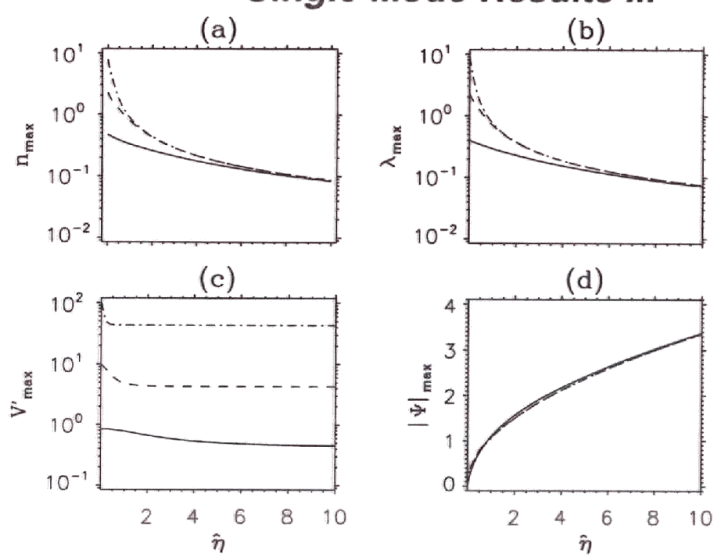

$\widehat{\Omega} = -2/3\widehat{\sigma}$, $v_A = \widehat{\nu} = 1$, and $\widehat{\sigma} = -100, -10, -1$ (dashed-dot, dashed, solid)

- For small $\widehat{\eta}, \widehat{\nu}$ MRI grows on dynamical timescale. As $\widehat{\eta}$ increase growth and wavenumber decrease but saturation levels in $|\Psi|$ increase.
- Behaviour consistent with the idea that reconnection reduces the effect of Lorentz force and thus enhance amplitude of MRI. This does not translate into increased V' (*i.e.* modification of background shear).

Approach to Saturated State

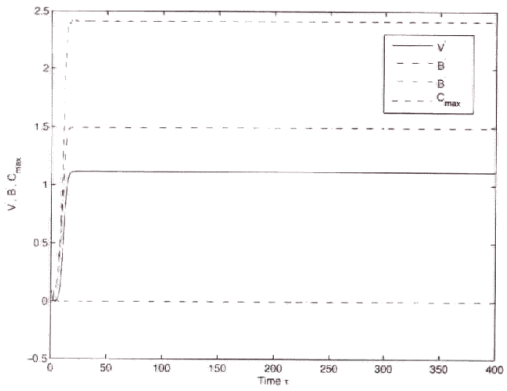

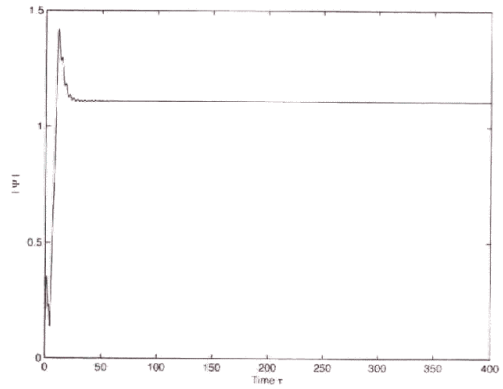

- Time-dependent evolution for x-invariant single-mode perturbation indicates approach to predicted stationary solutions.
- Above results display extreme cases, disks supported entirely by mechanical $(B' = 0)$ or magnetic $(B' \neq 0$ pressure.
- $\nu_t = 2\pi\epsilon|\Psi| \sim \mathcal{O}(\epsilon)$: turbulent viscosity associated with developed MRI.

Simulation of Full PDE

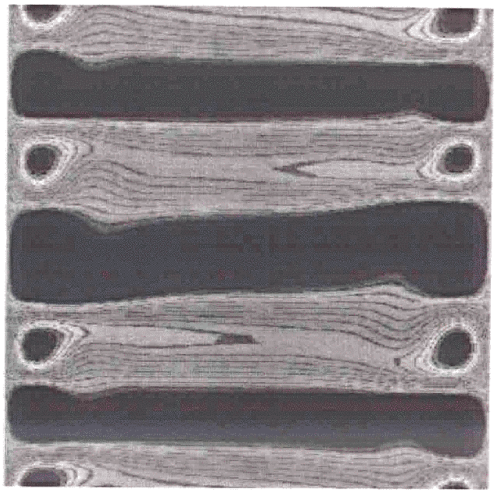

$\widehat{\Omega} = -2/3\widehat{\sigma}$, $\widehat{\sigma} = -4$, $v_A = \widehat{\nu} = \widehat{\eta} = 1$, and $\epsilon = 0.1$

- For impenetrable bc's, interior flow approaches x-invariant state.
- Inclusion of boundary layers requires extension of theory.

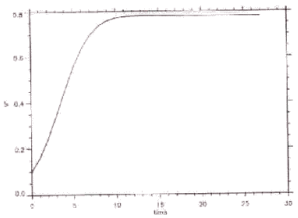

Figure 1. The evolution of $V'(X)$ for $\widehat{\sigma} = -1$, $\widehat{\Omega} = -2/3\widehat{\sigma}$, $\widehat{\eta} = 1$, $\widehat{\nu} = 1$, $v_A = 1$, and $\delta = \epsilon = 0.1$. Kinematic growth in the early phase is followed by saturation.

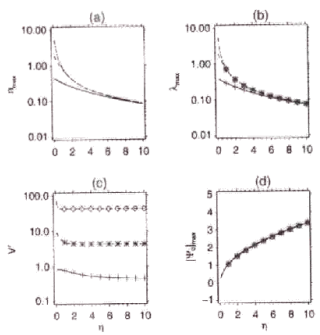

Figure 2. Comparison with single-mode theory. (a) The wavenumber n_{max} of the fastest growing mode, (b) its growth rate λ_{max}, (c) the resulting shear rate V'_{max} and (d) stream function amplitude at the midpoint $|\Psi_0|_{max} = \max_{0 \le z \le N_z L} |\psi'_{00}(L_x/2, z, t_{saturated})|$, as functions of $\widehat{\eta}$ for $\widehat{\Omega} = -2/3\widehat{\sigma}$, $\widehat{\nu} = 1$, $v_A = 1$ and $\widehat{\sigma} = -100, -10, -1$ (dashed-dot, dashed, solid). The numerical results with diamonds, asterisks and crosses representing $\widehat{\sigma} = -100, -10, -1$, respectively, are superposed on the analytical predictions of Knobloch & Julien [17]. The choice of the computational domain to be an exact multiple of the fastest growing wavelength ensures that the wavenumber is the analytically calculated n_{max}.

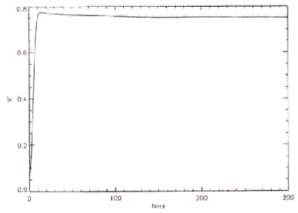

Figure 3. The evolution of $V'(X)$ with stress-free boundary conditions when $\widehat{\sigma} = -1$, $\widehat{\Omega} = -2/3\widehat{\sigma}$, $\widehat{\eta} = 1$, $\widehat{\nu} = 1$, $v_A = 1$, and $\delta = \epsilon = 0.1$.

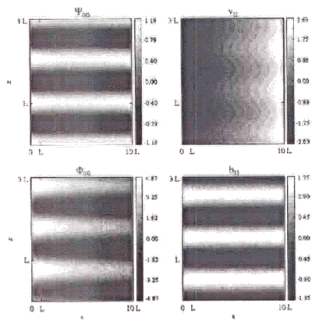

Figure 4. The saturated state reached in figure 3.

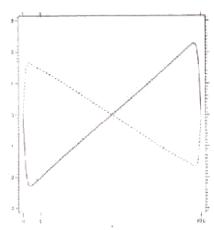

Figure 5. The z-average of v'_{11} (solid) and ϕ'_{00} (dashed) in figure 4. The quantities ψ'_{00} and b'_{11} have zero mean in the z direction.

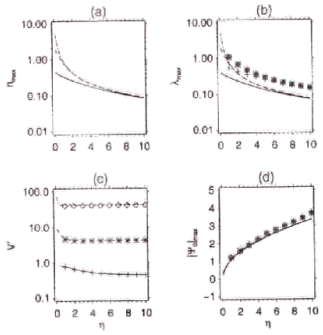

Figure 6. Asymptotic predictions for (a) the wavenumber n_{max} of the fastest growing mode, (b) its growth rate λ_{max}, (c) the resulting shear rate V'_{max} and (d) stream function amplitude at the midpoint $|\Psi_0|_{max} = \max_{0\le z\le N_z L} |\psi'_{00}(L_x/2, z, t_{saturated})|$, as functions of $\widehat{\eta}$ for $\widehat{\Omega} = -2/3\widehat{\sigma}$, $\widehat{\nu} = 1$, $v_A = 1$ and $\widehat{\sigma} = -100, -10, -1$ (dashed-dot, dashed, solid) with superposed numerical results (squares, diamonds, asterisks). The choice of the computational domain to be an exact multiple of the fastest growing wavelength ensures that wavenumber is the analytically calculated n_{max}.

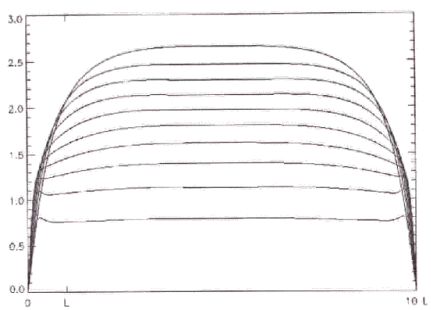

Figure 7. Root-mean-square ψ'_{00} as a function of $\widehat{\eta}$ for integer values from $\widehat{\eta} = 1$ (lowest curve) to $\widehat{\eta} = 10$ (highest curve) with $\widehat{\Omega} = -2/3\widehat{\sigma}$, $\widehat{\sigma} = -1$, $\widehat{\nu} = 1$, $v_A = 1$ and $\delta = \epsilon = 0.1$.

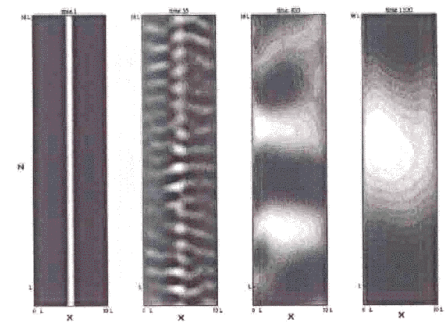

Figure 8. Evolution ϕ_{00} from an initial Gaussian profile in x with $\widehat{\sigma} = -1$, $\widehat{\Omega} = -2/3\widehat{\sigma}$, $\widehat{\eta} = 1$, $\widehat{\nu} = 1$, $v_A = 1$, and $\delta = \epsilon = 0.1$.

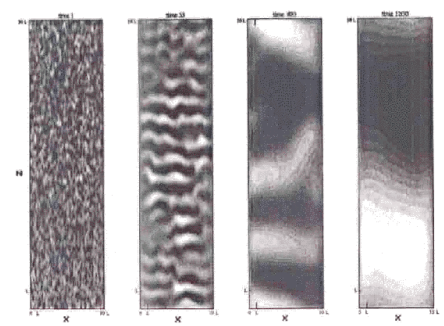

Figure 9. Evolution of ϕ_{00} starting from small amplitude random initial conditions with $\widehat{\sigma} = -1$, $\widehat{\Omega} = -2/3\widehat{\sigma}$, $\widehat{\eta} = 1$, $\widehat{\nu} = 1$, $v_A = 1$, and $\delta = \epsilon = 0.1$.

A Reduced Model for the MRI: Derivation and Simulation 16

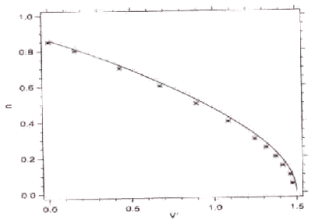

Figure 10. The value of $V'(X)$ for each of the saturated states begun with varying vertical box length L_Z, where $n = 2\pi/L_Z$. The solid line represents the single mode theory from [11], while the asterisks denote numerical results taken after the flow has coarsened to the box-filling wavelength (L) starting from a random small amplitude perturbation. The parameters are $\widehat{\Omega} = 1$, $\widehat{\sigma} = -1.5$, $\widehat{\nu} = \widehat{\eta} = 1$, $v_A = 1$ and $\delta = \epsilon = 0.1$.

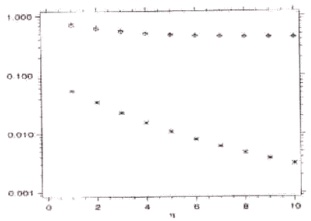

Figure 11. Reynolds and magnetic Reynolds stresses in (20) for $V'(X)$. The values of $V'(X)$, $-v_A^2\overline{a_{00}b_{11}}/\widehat{\nu}$, $\overline{u_{00}v_{11}}/\widehat{\nu}$ are represented by crosses, diamonds and asterisks, respectively. Here η varies from 1 to 10 while $\widehat{\sigma} = -1$, $\widehat{\Omega} = -2/3\widehat{\sigma}$, $\widehat{\nu} = 1$, $v_A = 1$, and $\delta = \epsilon = 0.1$.

Summary

- Simple scaling suffices to characterize one-parameter family of self consistent equilibrated states
  - Strong modification of background shear the feeds the MRI
  - Equilibration utimately determined by ohmic + viscous dissipation
- Comparison with Shearing Sheet simulations (BH 1991, HGB 95, Sano *et al.*98)
  - With resistive effects included and viscosity excluded unable to reach saturation. Theory indicates viscosity plays an equally important role.
  - MRI speed $\approx v_A \sim \mathcal{O}(1)$. Our theory indicates that the MRI saturates and flow speed is $\mathcal{O}(1)$ but independent of v_A. This is consistent with onset being independent of B_{pol}.
  - Simulation show tendency to solid body rotation and increased wavelength of MRI. This is also consistent with theory.
- publ's: Phys. Fluids 17, 094106 (2005); EAS Publications Series, 21 (2006); J. Math. Phys. 48, 065405 (2007).

RESULT OF SHEARING SHEET CALCULATION:

1) $v_t \sim u\ell = o(\varepsilon)$

2) $\ell \nearrow$ as $V' \nearrow$

3) both ν, η are required for saturation

4) exact, nonlinear but laminar solution

5) is the saturated state stationary?

$\lambda_{MRI} \ll \lambda_{healing}$: stationary (?)

$\lambda_{MRI} \gg \lambda_{healing}$: time-dependent (?)

6) consistency with 'imposed' Kepler shear

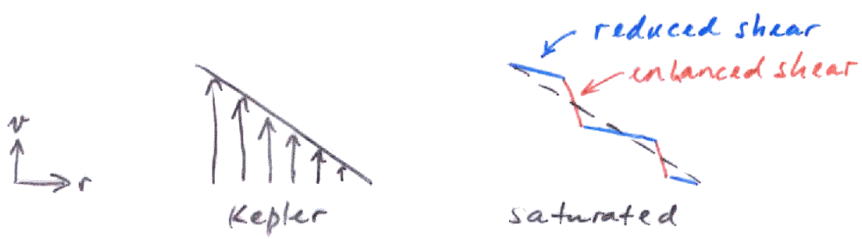

7) global aspects: azimuthal $\underline{B}$ and hoop stresses